



Non-oxidative methane conversion using lead- and iron-modified

albite catalysts in fixed-bed reactor

Ye Chen^{a,b,&}, Xin Wang^{a,b,&}, Xuegang Luo^b, Xiaoyan Lin^{a,b}, Yu Zhang^{b,*}

^a*Department of Materials Science and Engineering, Southwest University of Science and Technology, Mianyang 621010, Sichuan, China*

^b*Engineering Research Center of Biomass Materials, Ministry of Education, Mianyang 621010, Sichuan, China*

Abstract: Raw and modified albite catalysts, including Pb/Albite and Fe/Albite catalysts, have been investigated for methane conversion to C₂ hydrocarbons under non-oxidative conditions. Introduction of Pb to albite improved the activity and selectivity to non-coke products. Based on characterization, it was found that Pb entered into the alkali and alkaline-earth metal sites of albite, while partial Fe doped in the tetrahedron sites and the other loaded on the surface of albite. At the reaction temperature of 1073 K, methane gas hourly space velocity (GHSV) of 2 liter·gcat⁻¹·h⁻¹, catalyst dosage of 0.25 g (300 mesh), the methane conversion catalyzed by raw albite in the fixed-bed micro reactor exhibited a methane conversion of 3.32%. Notably, introducing a Pb content of 3.4wt% into albite greatly enhanced the conversion of methane up to 8.19%, and the selectivity of C₂ hydrocarbons reached to 99% without any coke under the same reaction conditions. While Fe-doping could weakly heighten the methane conversion to 3.97%, and coke was formed. Thus, a comparison of Pb/Albite and Fe/Albite catalysts demonstrates that the catalytic activity of albite is mainly decided by alkali and alkaline-earth metal sites, and lead-modification can effectively improve the catalytic activity of albite.

*Corresponding author.

E-mail address: zhangyuswust@163.com.

&These authors contributed equally to this work and should be considered co-first authors.

This article has been accepted for publication and undergone full peer review but has not been through the copyediting, typesetting, pagination and proofreading process, which may lead to differences between this version and the Version of Record. Please cite this article as doi: 10.1002/cjoc.201700800

Keywords: Methane conversion; Albite; C₂ hydrocarbons; Active site; Lead-modification

1. Introduction

The conversion of natural gas (typically 75% by weight methane) into other valuable higher hydrocarbons, including C₂ hydrocarbons, is of significant importance to the petrochemical industry. Being an important chemical raw material, C₂ hydrocarbons are increasingly demanded in both developed and developing countries. Including ethylene, the most produced organic compound in the world [1], C₂ hydrocarbons have a large market and can be obtained by direct conversion of methane [2-4]. Methane is an elementary building block for organic synthesis, and considerable interest has been paid to convert methane into more commercially useful C₂ hydrocarbons. Therefore, how to activate CH₄ and realize the conversion into high value-added products under mild conditions has become one of the most challenging subjects in the field of chemical industry [5,6].

In order to solve the problem, several different approaches based on catalysis and reaction engineering have been proposed and tested. Oxidative coupling of methane (OCM) [7] is a promising direct route for the production of C₂ hydrocarbons by oxidation of methane, which is thermodynamically feasible (exothermic process). However, the active sites in the coupling catalysts also activate the C-H bond in C₂H₆ and C₂H₄ and result in the formation of CO₂ by combustion, which leads to a low selectivity towards C₂ (50%-55%) and high selectivity of CO and CO₂ [8]. With respect to a higher selectivity of C₂ hydrocarbons, methane can be converted to C₂ hydrocarbons by the direct pyrolysis: $2\text{CH}_4 \rightarrow \text{C}_2\text{H}_6 + \text{H}_2 \rightarrow \text{C}_2\text{H}_4 + 2\text{H}_2 \rightarrow \text{C}_2\text{H}_2 + 3\text{H}_2 \rightarrow 2\text{C} + 4\text{H}_2$ [9,10]. According to the thermodynamics, the methane cracking is weak at the temperature of 1300 K below, and when the temperature increase to 2000 K above, methane can be pyrolyzed to

ethyne with a yield up to 85% [11]. Nevertheless, the increasing pyrolysis temperature will raise the cost and is not conducive to industrialization. Fortunately, the cracking temperature of methane can be reduced by adding suitable catalysts to activate the C-H bond [12], just as the catalyst showed in this paper. Compared with these two approaches, non-oxidative conversion of methane to C₂ hydrocarbons (NOCM) firstly defined by Belgued et al [13]. in 1990 avoids the deep oxidation of the products without CO or CO₂ and has achieved the direct and efficient conversion of methane to ethane, so the process has attracted the attention of many researchers [14,15].

The catalysts utilized for NOCM are usually over monometallic catalysts that are composed of or modified by compounding them together [16,17], where metals include precious metals, rare-earth metals and transition metals, including Ru, Co [18], Re [19], Pt [20], Pd [21], and Ni [22], then Al₂O₃ [23], SiO₂ [24] and molecular sieve [25] are applied as general carriers. Unfortunately, accumulation of coke on the catalyst surface results in deactivation and loss of selectivity from 91% to 66% [23].

Up to date, the study of the single-atom active center catalyst has become one of the new frontiers and hotspots in the field of catalysis [26]. The NOCM to C₂ hydrocarbons can be catalyzed by single site catalyst, which is generally supported catalyst [27]. As a result, the active components are not stable under the condition of high temperature and easy to coke. Accordingly, the reaction temperature should be below 873 K, which leads to methane conversion occurs at a fairly low rate (<1%) [13]. Unlike the supported catalysts, Xinhe Bao et. al achieved a high efficient conversion of methane under high temperature by the construction of Fe-Si bond in Fe@SiO₂, a single-atom active center catalyst, which did not deactivate in an 60-hour test [28]. In a word, without any coke deposition, the catalytic activity of the catalyst can be heightened through

the construction of the single-atom active center catalyst, which probably solve the problem of NOCM catalyst.

Based on above, a new catalyst for NOCM, which is employed under mild conditions and do not produce any coke, has been considered in this paper. Albite, a natural mineral with a chemical formula of $A[T_4O_8]$ (major elements shown in Table 1), was studied as a catalyst for NOCM here [29]. Albite consists of vertex-shared $[SiO_4]$ and $[AlO_4]$ tetrahedra that form tetra-atomic and octatomic rings tunnels. Cationic Na(I), K(I), Ca(II), Mg(II) and so on occupy the interspace between the tetra-atomic ring, forming A site (see Fig. 1) [30]. Owing to the natural structural properties of albite, the alkali and alkaline-earth metal sites have not only positive and negative charge attraction with $[TO_4]$ (T=Al, Si), but also a induced force with the oxygen bridge, so it can keep stable at the high temperature. Alkali and alkaline-earth metal sites (A sites) can be ion-exchanged with metal ions of large radius, offering a variety of possible active sites for methane activation. Importantly, albite has a good cleavage in the direction of parallel to the chain. As a result, it is likely that alkali metal sites are exposed on the external and become active, which may directly contact with methane molecular to catalyze NOCM. In theory, alkali and alkaline-earth metal sites in albite are the steady sites of coordinatively unsaturated metal center, and can be introduced into reactive metal by ion-exchange to form the active center for NOCM.

Table 1. The ionic radius of the major elements in albite.

Site	T site		A site			
Element	Si (IV)	Al (III)	K (I)	Na (I)	Ca(II)	Mg (II)
Radius(nm)	0.034	0.047	0.159	0.124	0.120	0.097

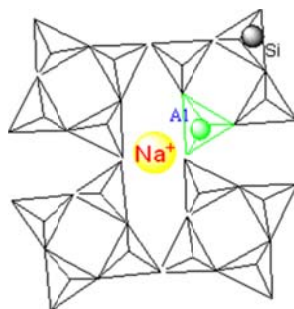


Fig. 1 Basic structure of albite.

This paper is devoted to the catalytic performance study of albite, and Pb and Fe elements with higher activity were applied to make albite modified. The catalytic test of raw and modified albite in the NOCM to C₂ hydrocarbons was studied, which exhibits higher selectivity (>99%), activity, and stability for production of C₂ hydrocarbons without any coke. For comparison purpose, the structure, the morphology and the catalytic property of Pb- and Fe-modified albite catalysts for NOCM were examined in order to find the acting active site for non-oxidative methane conversion.

2. Experimental

2.1 Reagents

The Pb/Albite (Pb/Ab) and Fe/Albite (Fe/Ab) catalysts were prepared by calcination in Muffle furnace (SXW-5-17Z, Shanghai, China). Albite (100 mesh, Hebei, China), PbCl₂ (AR, Kelon Chengdu, China), Fe₂O₃ (Nano-scale, Aladdin, Shanghai, China), HF (39%, Kelon, Chengdu, China), deionized water (laboratory homemade) were used in catalyst preparation.

2.2 Catalyst preparation

2.2.1 Pb/Ab catalyst

In a typical procedure, foremost the albite powder was calcined at 1373 K for 5 h to eliminate impurities in natural albite (see Fig. S1 in Supporting Material). Then it was milled in the ball mill

(QM-1SP2, Nanjing, China) with a speed of 5000 r/min for 2 h to obtain the fine albite powder (300 mesh). Afterwards, special amount (mass ratio of PbCl_2 /albite was 0.1, 0.5 and 1) of PbCl_2 was mixed with the albite powder. After an intermediate grinding, the powder was further calcined at 773 K for 25 h in air to finish ion-exchange. Then the powder was adequately washed to remove redundant PbCl_2 and finally dried in an oven at 383 K to obtain the final Pb/Ab catalyst.

2.2.2 Fe/Ab catalyst

To be brief, special amount (depends on the specific catalyst; e.g. mass fraction of Fe was 0.5, 1 and 3 wt%) of nano-scale Fe_2O_3 was mixed with albite. Then the mixture was milled in the ball mill with a speed of 5000 r/min for 2 h. Subsequently, the powder mixture was calcined at 1373 K in air for 5 h to dope Fe into albite. After being crashed into 50-100 mesh by using universal high-speed smashing machines (FW-80, Beijing, China), the powder was grinded into 300 mesh in a mortar to obtain the final Fe/Ab catalyst.

2.3 Catalyst characterization

A series of ion-changed Pb/Ab catalysts were detected by inductively coupled plasma spectra (ICP) (Agilent, 7700x) to measure the content of ion exchange between Pb and Na in albite. The test conditions were RF power of 1450 W, pump speed of 0.1 rpm, atomizing chamber temperature of 2 °C, sampling depth of 8.0 mm, plasma gas flow rate of 15 L/min and nebulizer gas flow rate of 0.75 L/min. Before measurement, all the obtained catalysts powder was digested using HF acid according to the method in literature [31].

To determine the coordination state of the iron element, Fe/Ab catalysts were measured by Brook EMX-10/12 Electron spin resonance (ESR) spectrometer with an operating frequency of 9.76 MHz.

The phase characterization of raw and modified albite catalysts were analyzed by X-ray diffraction (XRD) analysis on a Panalytical X'Pert PRO diffractometer (The Netherlands). The samples were scanned from 10 to 60° 2 θ . Cu K α radiation ($\lambda = 0.15406$ nm) generated at 40 kV and 30 mA was used as the X-ray source.

X-ray photoelectron spectroscopy (XPS) (Thermo SCIENTIFIC ESCALAB 250, USA) analysis was performed to estimate the surface composition and binding energy between atoms of catalysts. The instrument was equipped with a monochromatic Al K α radiation source operated at a power of 300 W. The binding energy was calibrated using the adventitious carbon (C 1s peak at 284.6 eV).

The morphology of modified albite was observed by Libra 200FE field emission transmission electron microscopy (TEM), with an acceleration voltage of 200 KV.

The total amount of coke accumulated in the spent catalysts was obtained from the weight loss in the 50-1050 K range determined by thermogravimetric analysis (TGA) in a TQ500 equipment under a flow of air and heating from room temperature to 1050 K at a rate of 10 K/min.

2.4 Catalyst testing

The catalytic NOCM reaction was implemented at 873-1073 K and atmospheric pressure in a fixed-bed flow reactor (see Fig. S2 in Supporting Information). Specifically, 0.25 g of Pb/Ab or Fe/Ab catalyst (300 mesh) was mixed with 2 g quartz sand (50-100 mesh), then the mixture was filled in the middle of quartz tube (7 mm.i.d.) and both ends were fixed with silica wool. Firstly, the catalyst was heated to a predetermined temperature with a speed of 4 °C/min at air atmosphere, then the feeding gas (90vol% CH₄/10vol% Ar) was continuously injected at a determined gas hourly space velocity (GHSV) for 0.5 h as prereaction. After that, it was time to collect the reaction

gas. Subsequently the reaction gas was analyzed by Agilent7890A gas chromatography (GC) equipped with FID detector and PLOT-Q capillary column. The activity of the Pb/Ab and Fe/Ab catalysts was characterized by the yield of C₂ hydrocarbons.

2.5 Analysis

The percentage of various components of the reaction gas was obtained by normalization method [32,33], the formula is as follows:

$$X_i = A_i \times f_i \quad (1)$$

Where X_i is the molar concentration of chemical i, A_i represents the peak area of chemical i, and f_i is the correction factor of chemical i.

Methane conversion is given:

$$CH_{4(conv)} = \frac{X_{CH_4(bef)} - X_{CH_4(af)}}{X_{CH_4(bef)}} \times 100\% \quad (2)$$

Where $CH_{4(conv)}$ is the conversion of methane, $X_{CH_4(bef)}$ and $X_{CH_4(af)}$ are the initial and final molar concentration of methane, respectively.

Selectivities of C₂ hydrocarbons are as follows:

$$C_2H_{6(sel)} = \frac{2 \times X_{C_2H_6}}{X_{CH_4(bef)} - X_{CH_4(af)}} \times 100\% \quad (3)$$

$$C_2H_{4(sel)} = \frac{2 \times X_{C_2H_4}}{X_{CH_4(bef)} - X_{CH_4(af)}} \times 100\% \quad (4)$$

$$C_2H_{2(sel)} = \frac{2 \times X_{C_2H_2}}{X_{CH_4(bef)} - X_{CH_4(af)}} \times 100\% \quad (5)$$

$$C_{2(sel)} = C_2H_{6(sel)} + C_2H_{4(sel)} + C_2H_{2(sel)} \quad (6)$$

Where $C_2H_{6(sel)}$, $C_2H_{4(sel)}$, $C_2H_{2(sel)}$, and $C_{2(sel)}$ represent the selectivity of ethane, ethylene, ethyne, and C₂ hydrocarbons, respectively; $X_{C_2H_6}$, $X_{C_2H_4}$, and $X_{C_2H_2}$ are the molar

concentration of ethane, ethylene and ethyne, respectively.

Yield of C_2 hydrocarbons is as below:

$$Y_{C_2} = CH_{4(\text{conv})} \times C_{2(\text{sel})} \quad (7)$$

Where Y_{C_2} is the yield of C_2 hydrocarbons.

The quantitative method of coke amount is as below [34].:

$$\text{Coke amount} = \frac{m_i - m_f}{m_i} \times 100\% \quad (8)$$

Where m_i represents the weight of coked catalyst after desorption of water and m_f represents the weight of coked catalyst after burning off the coke

Carbon balance is as below [35]:

$$X_{CH_4(\text{Bef})} - X_{CH_4(\text{Aft})} = 2(X_{C_2H_6} + X_{C_2H_4} + X_{C_2H_2}) + X_{Coke} \quad (9)$$

Where Y_{Coke} is the molar concentration of coke.

3 Results and discussion

3.1 Catalyst characterization

3.1.1 Structure analysis

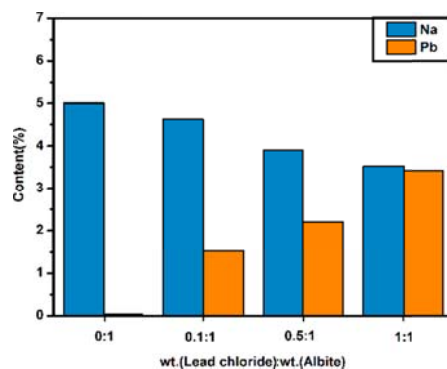


Fig. 2 ICP results of ion-exchanged albite with different mass ratios of lead chloride and albite.

The contents of Pb(II) and Na(I) in albite can be observed intuitively from ICP results in Fig.

2. As seen, when the mass ratios of lead chloride and albite were 0, 0.1, 0.5 and 1, Na(I) contents

were 5.0, 4.6, 3.9 and 3.5wt% and Pb(II) contents were 0.1, 1.5, 2.2 and 3.4wt%, respectively. It is determined that the content of Na(I) decreases along with the increase of Pb(II) content, which is speculated that Na(I) was exchanged by Pb(II). In fact, in silicate mineral albite, alkali or alkaline-earth metal ions will be compensated the excess negative charges generated when partial Si(IV) are replaced by Al(III). Balancing the electric interaction in the void, these cations can participate in the ion-exchange reaction at the condition of that the crystal structure of albite could not be destroyed due to the strong liquidity and small binding energy with crystal skeleton [36]. On the other hand, the ion-exchange reaction occurs between dissociative lead ions and sodium ions in albite in the vicinity of the melting point of lead chloride, resulting the production of soluble sodium and Pb/Ab. Followed by the formation of Pb/Ab, the structure of albite is still not damaged, which is consistent with the results of previous study [37].

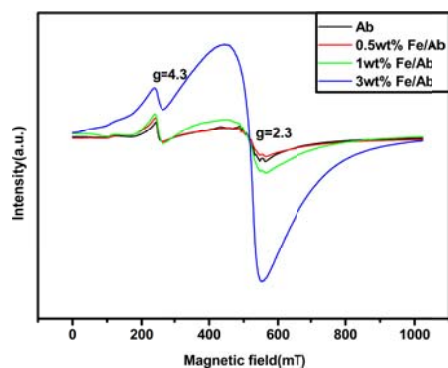


Fig. 3 ESR spectra of Fe/Ab with different Fe contents.

The transition metal ions with unpaired electron have paramagnetic effect, and different coordination states can cause difference of the ESR spectra of the fine structure. According to the study of the paramagnetic iron atom, the coordination situation of iron atoms in albite can be judged from the spectral split factor g . Two obvious signals appear in ESR spectra (Fig. 3), which are attributed to the Fe(III) of the coordination of four and eight at $g=4.3$ and 2.3 , respectively [38].

It is depicted that the intensities of the two absorption peaks increase with the increasing Fe (III) content, and the peak height of $g=2.3$ significantly increases at 3wt%Fe. Especially, it might be illustrated that the absorption peak of $g=4.3$ shows partial iron atoms doped into the albite framework $[TO_4]$, forming a tetrahedral structure [39].

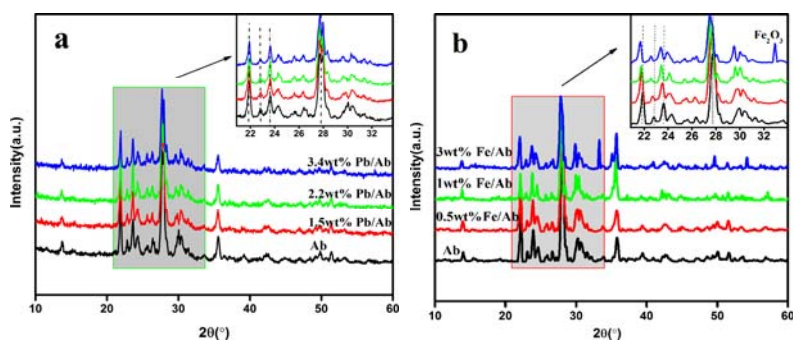


Fig. 4 XRD spectra of modified albite with different metal contents. (a) Pb/Ab; (b) Fe/Ab.

XRD spectra of Pb/Ab and Fe/Ab catalysts with different Pb or Fe contents are depicted in Fig. 4. As shown in Fig. 4a, the typical diffraction peaks at $2\theta=20^{\circ}-34^{\circ}$ indicates that the framework of the albite was still retained without obvious changes of relative crystallinity in all the samples, which can be indexed to pure albite $Na(AlSi_3O_8)$ (JCPDS 99-0001). Furthermore, the absence of peak of lead chloride or lead oxide indicates that Pb(II) was well dispersed in albite and did not appear in the albite framework so that it had no effect on albite structure. In this sense, lead element successfully entered into the A site of the albite $A[T_4O_8]$, and achieved the purpose of ion exchange, which has borne out the ICP analysis.

In different iron-doped proportions, XRD spectra of albite did not change obviously (Fig. 4b), which can be indexed to pure Albite $Na(AlSi_3O_8)$ (JCPDS 99-0001). A comparison of the albite spectra with different iron contents demonstrates that the diffraction peaks of Fe/Ab shift toward the lower angle followed the iron content increasing. As report goes, when the heteroatom of larger radius than Al and Si atom was introduced in the molecular sieve, heteroatom in molecular sieve

framework often caused lattice constants and unit cell volume become larger, resulting in that the diffraction peaks of the sample shifted to lower angles than that of the undoped sample [40]. In effect, albite and molecular sieve are both connected with silicon-oxygen or alumina-oxygen tetrahedrons, so the diffraction peaks of Fe/Ab shifted toward the lower angle direction. This further shed light on that Fe element successfully entered into the albite framework $[TO_4]$. Specifically, only some of iron oxide doped into the tetrahedron framework $[TO_4]$ in albite and the other failed, which is obvious for the new peak at 33.2° in XRD attributed to iron oxide (JCPDS 89-0599) in the spectrum of 3wt% Fe/Ab. This may be due to that the melting point of iron oxide (1838 K) is much higher than that of albite (1373 K), resulting that partial iron oxide can not fully melt into albite at 1373K.

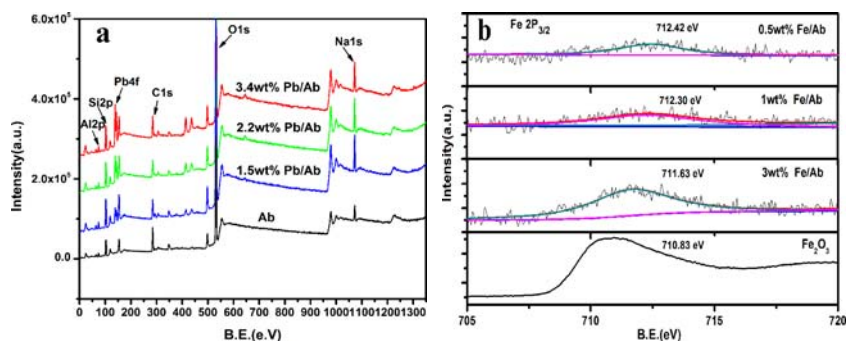


Fig. 5 XPS patterns of modified albite with different modified-metal contents. (a) Pb/Ab; (b) Fe/Ab.

Fig. 5 demonstrates the XPS patterns of Pb/Ab and Fe/Ab catalysts with different Pb or Fe contents. As shown, the peaks at 138.9 eV and 1072.1 eV should be attributed to Pb $4f_{7/2}$ and Na 1s, respectively (Fig. 5a). Of these, the peak of Pb $4f_{7/2}$ at 138.9 eV is close to that of lead silicate. It can be observed that the peak intensity of Pb $4f_{7/2}$ increases while Na 1s decreases. In combination with ICP and XRD analysis, it is again verified that Pb(II) successfully ion-exchanged with Na(I) in albite and entered into alkali metal site of albite [37,41].

The Fe $2P_{3/2}$ peak position of the albite moves to the direction of high binding energy, and the

lower the doping amount, the greater the amplitude of the shift (Fig. 5b). It is an obvious signal that Fe successfully doped into the albite framework. This shift can be attributed to that Si(IV) is more electronegative than Fe(III), resulting in an induced effect on Fe(III) by bridging oxygen bond. As a consequence, the electric potential energy of skeleton Fe(III) increased, leading to the increase of electron binding energy of skeleton iron. It is further corroborated that partial iron oxide is successfully incorporated into T site of albite [41]. On the other side, the peak position of Fe $2P_{3/2}$ is closer to that of Fe_2O_3 when the iron content reached 3wt%. Combining with the results of ESR and XRD analysis, it may be ascribed to that after Fe-doping partial iron oxide did not enter into the albite tetrahedron framework $[TO_4]$, which is more obvious in spectra of 3wt%Fe/Ab catalyst.

3.1.2 Morphology analysis

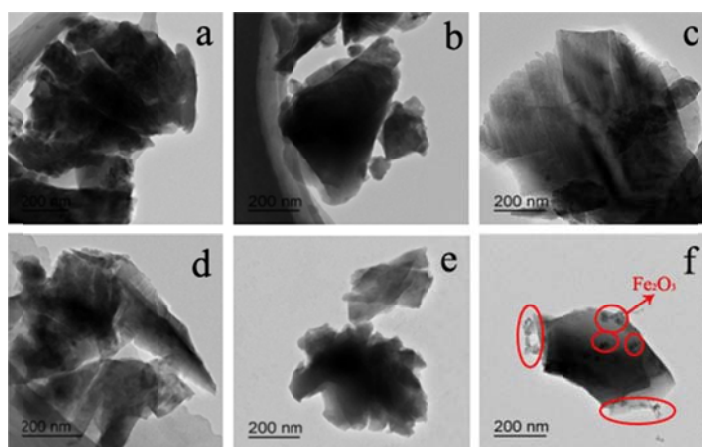


Fig. 6 TEM patterns of modified albite with different modified-metal contents. (a) 1.5wt% Pb/Ab; (b) 2.2wt% Pb/Ab; (c) 3.4wt% Pb/Ab; (d) 0.5wt% Fe/Ab;(e) 1wt% Fe/Ab;(f) 3wt% Fe/Ab.

TEM patterns of Pb/Ab and Fe/Ab catalysts with different modified-metal contents are shown in Fig. 6. As depicted in Figs. 6a, b and c, the morphologies of 1.5, 2.2 and 3.4wt%Pb/Ab catalysts have no clear change and are still a plate structure, without other attachments on the surface after high content of Pb modification. This result is in agreement with the conclusion above.

Apparently, 0.5 and 1wt%Fe/Ab is still a plate structure (Figs. 6d, e), which is accord with the

flaky dissociation of albite. The obvious appearance of spherical particle on the surface of 3wt%Fe/Ab indicates that partial iron oxide did not melt into albite and loaded on the surface of albite (Fig. 6f). This is consistent with the XRD results, and also corroborates the reason why XPS diagram of Fe 2P_{3/2} peak of 3wt%Fe/Ab moved to lower binding energy direction is that partial iron oxide failed to enter into albite. Thus, it is reliably ascertained that partial iron oxide did not enter into the albite framework [TO₄] after Fe-doping, which can be intuitively reflected in 3wt%Fe/Ab catalyst.

Compared with the characterization of Pb/Ab and Fe/Ab catalysts, it was found that Pb(II) smoothly entered into A site of albite, while partial Fe(III) successfully doped into T site of albite and the remaining loaded on the surface of albite.

3.2 Catalytic performance on NOCM

3.2.1 Study on catalytic properties of albite

First of all, the catalytic effects of raw albite under different temperatures and space velocities were investigated, which are depicted in Fig. 7. The albite dosage was 0.25 g, and the reaction time was 1 h.

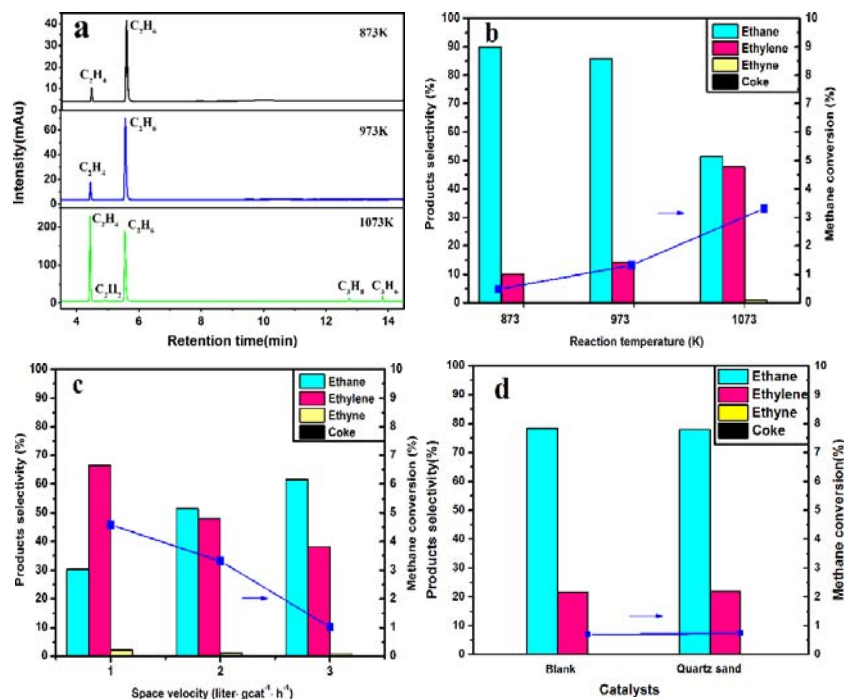


Fig. 7 Catalytic activity of raw albite with different conditions including (a) GC chromatography (b) temperatures ranging from 873 to 1073 K, (c) methane GHSV varied from 1 to 3 liter·gcat⁻¹·h⁻¹ at temperature of 1073 K. (d) catalytic performance of quartz sand at temperature of 1073 K and methane GHSV of 2 liter·gcat⁻¹·h⁻¹.

Fig. 7a shows the GC spectra of the products of methane conversion catalyzed by albite at different temperatures. Intuitively, the products contain C₂ hydrocarbons (ethane, ethylene and ethyne) and C₃ hydrocarbons (propane and propylene). Of these, ethane and ethylene were the main products. What's more, the content of C₃ hydrocarbons was so little that the study focus has been C₂ hydrocarbons in this paper.

Fig. 7b demonstrates the calculation results of GC pattern at Fig. 7a. As shown in Fig. 7b, the conversion of methane increased apparently from 0.86% to 3.32% followed the reaction temperature increasing from 873 K to 1073 K. This might be attributed to that the increasing reaction temperature improved the activity of catalytic site in albite, which was favor to methane conversion. Meanwhile, at the reaction temperature ranging among 873 K and 1073 K, ethane selectivity decreased from 90.1% to 51.4%, while ethylene selectivity increased from 9.9% to 47.8%

and ethyne selectivity increased from 0 to 0.6% without any coke. It might be ascribed that ethane is so unstable in high temperature that would further dehydrogenate to produce ethylene and ethyne [10]. Remarkably, the methane conversion at 1073 K was greatly higher than that of 973 K.

The effects of methane GHSV (from 1 to 3 liter·gcat⁻¹·h⁻¹) on the catalytic performance of albite for NOCM are depicted in Fig.7c. It can be seen that the conversion of methane decreased from 4.62% to 1.05% while the selectivity of C₂ hydrocarbons did not decrease obviously when methane GHSV increased from 1 to 3 liter·gcat⁻¹·h⁻¹ at temperature of 1073 K. Specifically, besides a bit of ethyne, the selectivity of ethane was improved from 30.4% to 61.6%, while the selectivity of ethylene decreased from 66.5% to 38.1%. This could be explained that when the feed gas spacevelocity increased, the residence time of the product gas in the high temperature region was shortened, so methane molecule had less time to be converted and the continuous dehydrogenation of C₂ hydrocarbons was weakened.

By comparison, a blank experiment (an empty reactor with no catalyst) under the same conditions showed a methane conversion of only 0.75% (Fig. 7d). A test with quartz sand as the catalyst yielded virtually the same result. Therefore, quartz sand had no obvious effect on methane conversion, and it can be mixed with finer albite powder to make methane gas pass through.

In conclusion, the best catalytic effect of raw albite for NOCM is that the methane conversion rate was up to 3.32% and the main products were ethane and ethylene without any coke at the optimal experimental conditions of the temperature of 1073 K, methane GHSV of 2 liter·gcat⁻¹·h⁻¹, reaction time of 1 h and catalyst dosage of 0.25 g.

3.2.2 Pb/Ab catalyst

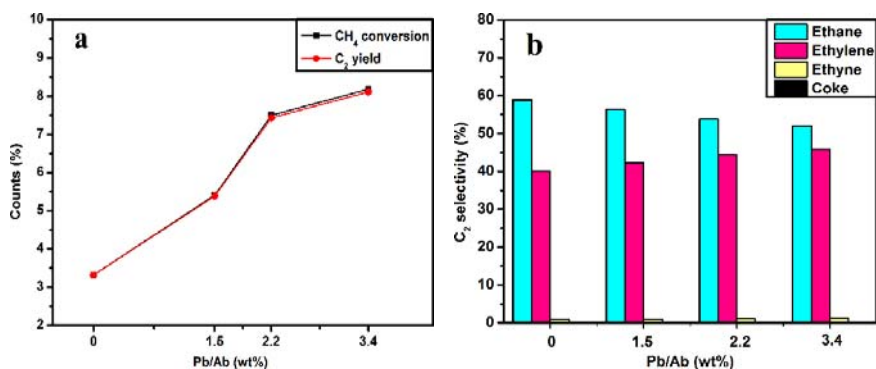


Fig. 8 Catalytic activity of Pb/Ab with different Pb contents. Reaction conditions: the reaction temperature of 1073 K, the methane GHSV of 2 liter·gcat⁻¹·h⁻¹, and the catalyst dosage of 0.25 g (300 mesh).

The NOCM tests of modified-albite were implemented under the optimal experimental conditions for the highest catalytic activity of albite. The results of catalytic activity test of Pb/Ab with different Pb contents are depicted in Fig. 8. As shown, when the Pb content increased from 0 to 3.4wt%, the conversion of methane increased from 3.32% to 8.19%. Meanwhile, C₂ hydrocarbons yield increased from 3.31% to 8.11% (Fig. 8a). It shows that Pb-modification can significantly enhance the catalytic activity of albite. Combined with the characterizations above, this may be attributed to that Pb(II), an ion with higher activity than Na(I), ion-exchanged with Na(I) to enter into A site and improved the catalytic activity of A site, which was favourable for methane activation.

Containing trace ethyne (about 0.2%), the main components of the C₂ hydrocarbons were ethane (about 53.4%) and ethylene (about 45.8%) after reaction (Fig. 8b). Fairly accurately, lead-modification could weakly improve the selectivity of ethylene, but the overall selectivity of C₂ hydrocarbons did not decrease, conforming the reaction process did not produce coke. This may be ascribed to that the ion-exchange between Pb(II) and Na(I) in A site of albite enhanced the activity of albite for methane conversion, but did not change the albite structure so that it had a little effect on the selectivity of C₂ hydrocarbons.

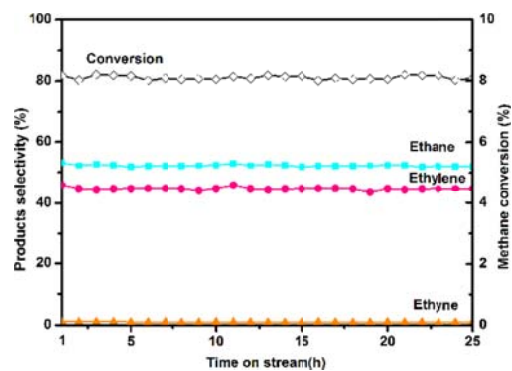


Fig. 9 The stability of Pb/Ab catalyst. Reaction conditions: the reaction temperature of 1073 K, the methane GHSV of 2 liter·gcat⁻¹·h⁻¹, and the catalyst dosage of 0.25 g (300 mesh).

Furthermore, the stability of Pb/Ab catalyst was tested. Fig. 9 shows the catalytic activity of albite for NOCM during the reaction time from 1 h to 25 h. Obviously, with the extension of reaction time, the conversion of methane and the selectivity of the ethane, ethylene and ethyne had only a small fluctuation and maintained at a stable value of 8.17%, 53.7%, 45.5% and 0.3%, respectively. This illustrates that Pb/Ab catalyst showed the relatively steady catalytic performance on NOCM.

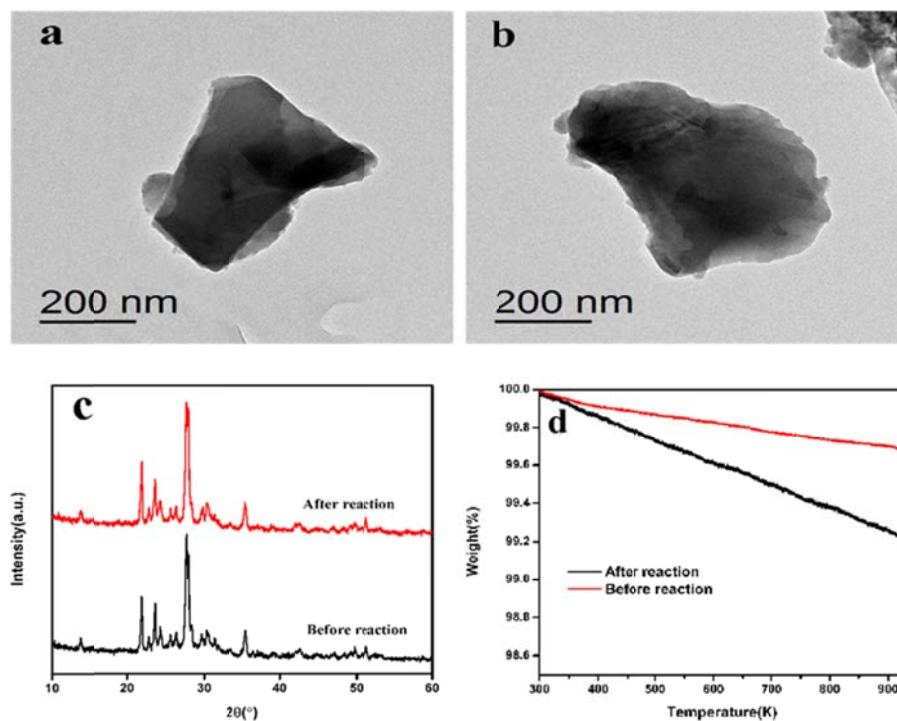


Fig. 10 TEM (a) (b), XRD (c) and TGA (d) spectra of Pb/Ab catalyst before and after reaction for 25 h.

The TEM image, XRD and TGA curves of Pb/Ab catalyst before and after reaction for 25 h were measured. The TEM image of the Pb/Ab catalyst after the reaction (Fig. 10a,b) shows that the morphology of the Pb/Ab catalyst did not change significantly after the reaction and remained a layered structure with no other attachments, demonstrating that no coke was produced. As can be seen from Fig. 10c, the XRD pattern of the Pb/Ab catalyst before and after reaction did not change significantly, indicating that no obvious structural changes occurred in the Pb/Ab catalyst during the NOCM reaction, and no carbon deposition occurred. Fig. 10d shows that the weight loss rate of Pb/Ab catalyst before reaction was 0.31% at 300 K-1050 K, and the weight loss rate of Pb/Ab was 0.73% after NOCM reaction for 25 h. It can be seen that there is such little change of the weight loss rate of Pb/Ab catalyst before and after 25 h reaction, so that it could be ignored. Meanwhile, there is no weight loss peak due to coking at around ~ 700 K and ~ 750 K [43,44]. Combined with XRD and TEM analysis results, it was indicated that Pb/Ab catalyst did not form coke during the reaction.

3.2.3 Fe/Ab catalyst

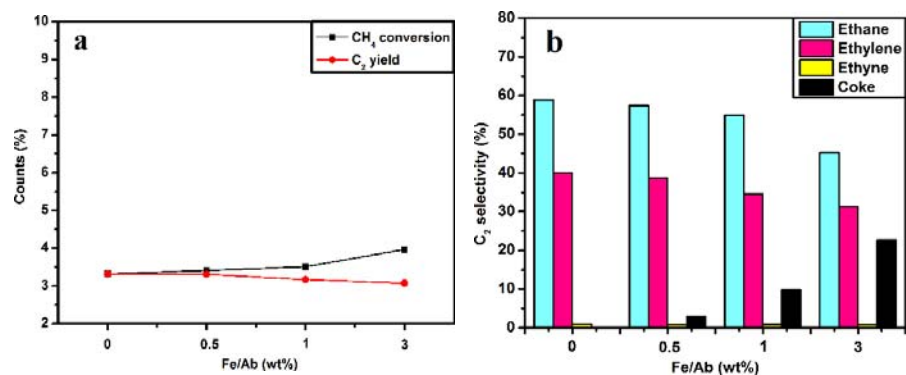


Fig. 11 Catalytic activity of Fe/Ab with different Fe contents. Reaction conditions: the reaction temperature of 1073 K, the methane GHSV of $2 \text{ liter} \cdot \text{gcat}^{-1} \cdot \text{h}^{-1}$, and the catalyst dosage of 0.25 g (300 mesh).

The conversion rate of methane increased slightly followed the iron-doping increasing (Fig.

11a). Specifically, the doping amount increased from 0 to 3wt% followed by the conversion rate of methane increased from 3.32% to 3.97%. Instead, the yield of C_2 hydrocarbons was reduced from 3.31% to 3.06%.

With a shred of ethyne, the main components of products were ethane, ethylene and coke (Fig. 11b). The selectivity of C_2 hydrocarbons gradually decreased from 99% to 75.6% followed iron-doping increasing from 0 to 3wt%. According to the characterization results above, it is attributed to that a part of iron oxide entered into the albite framework $[TO_4]$ and weakly raised the activity of albite for methane conversion. Meanwhile, the other part of iron oxide failed to enter into albite framework $[TO_4]$, but loaded on the surface of albite in the modification process, resulting the heavy coke production and the lower selectivity of C_2 hydrocarbons. This is conformed with the metal-doping catalysts, which were widely used in methane dehydrogenation to obtain nanocarbon and hydrogen [45-47].

3.3 Mechanism of NOCM

As dicussed above, albite has an obvious effect on the methane conversion under non-oxidative condition (Fig. 7). In order to enhance catalytic effect, two ions, Fe(III)(0.057 nm) and Pb(II)(0.137 nm), whose activities are higher than native ions in albite and radii are close to that of A and T sites in Table 1 were chosen to make albite modified at different sites.

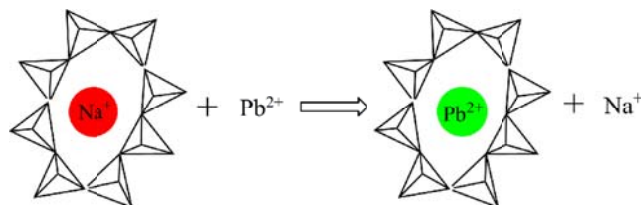


Fig. 12 Schematic diagram of alkali-metal sites modified.

Pb(II) substituted Na(I) in albite to enter into the alkali-metal site in the void between

octatomic ring, forming Pb/Ab catalyst, as shown in Fig. 12. With unoccupied d orbitals, a lead ion shows higher activity and can be coordinated by one Si (Al) and two methane molecules. In other words, Pb was introduced into alkali-metal site to form the Pb/Ab catalyst with higher catalytic activity, which greatly promoted the conversion of methane (Fig. 8). This further proves that the alkali and alkaline-earth metal sites are the active sites. On the one side, the tetra-atomic ring chain paralleling to the direction of chain elongation is stably combined in albite structure, so the crystal along this direction is not easily broken. On the other side, although oxygen bridge connection exists among chains perpendicular to the direction of chain growth, some rely on a coordination bond between metal ions and O^{2-} ions, so the combination is much weaker than that of the former. As a result, albite has a good cleavage in parallel to the direction of the chain (Fig. 6). Then alkali and alkaline earth metal ions will be exposed to the external of albite after cleavage, forming coordinatively unsaturated metal center to stably exist at high temperatures and become the center of methane activation, which has been proved in the catalyst characterization section.

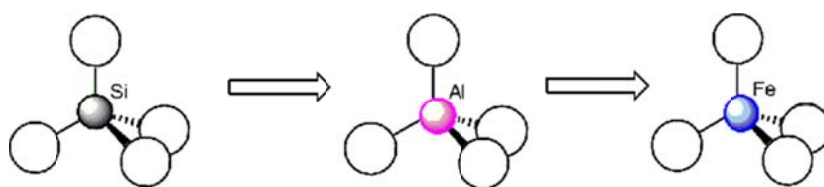
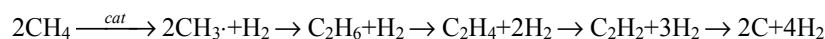


Fig. 13 Schematic diagram of modified $[TO_4]$ structure.

Fe, an element with higher activity than Na, partly doped into T site of albite framework $[TO_4]$ to form the Fe/Ab catalyst, which weakly promoted the conversion of methane (Fig. 11). It is implied that T site is not the active site of albite. Actually, reactants need to react with catalyst to be activated in heterogeneous catalytic reaction, and methane activation requires that the methane molecules are chemically adsorbed on the catalyst surface and needs the interaction between methane and metal site [19,25]. But in albite structure, each silicon or aluminum atom is

surrounded by four oxygen atoms, forming a silicon-oxygen or aluminum-oxygen tetrahedron (Fig. 13). So does the iron-oxygen tetrahedron[37]. Furthermore, with the smaller ionic radius than that of the surrounding oxygen, the intermediate silicon, aluminum and iron are completely coated by oxygen. Due to the intermediate metal site is closed by tetrahedral structure and methane molecules are unable to contact with the active metal, so that it can not be activated on the catalyst. Accordingly, $[TO_4]$ is clearly not consistent with such a structure, which could explain why the doping of transition metal iron did not significantly improve the activity of albite.

In this paper, the process of methane conversion occurred at the catalytic site of albite is similar to catalytic cracking of methane, which can be speculated based on the previous studies [9-11] and the experimental study. The possible reaction process is given:



First of all, alkali-metal sites of albite activates and initiates methane molecules dehydrogenation by generating methyl radicals at high temperature, and then ethane is generated by the combination of two methyl radicals [28]. Next, the dehydrogenation of ethane and its subsequent dehydrogenation at varied reaction temperatures and methane spacevelocites are consistent with the thermal decomposition process of alkanes. Ethane is so unstable at high temperature that continued to produce ethylene by dehydrogenation [10]. If the temperature continues to rise or the residence time of ethylene in high temperature area is lengthening, ethylene will continue to be converted into ethyne by dehydrogenation. Then coke is formed by the dehydrogenation of ethyne, which is only present in Fe/Ab catalyst due to the poorly dispersed iron oxide.

4. Conclusion

Here we show that albite can be employed in methane conversion under non-oxidative conditions. The conversion of methane catalyzed by raw albite was 3.32%. After introducing a Pb content of 3.4wt% to albite, a conversion as high as 8.19% was obtained at 1073 K and a space velocity of 2 liter gcat⁻¹ hour⁻¹, with a selectivity to C₂H₄ of 47.4%. It is worth mentioning that the Pb/Ab catalyst as a single-active-center-like catalyst exhibited a higher performance on NOCM than conventional catalysts, due to that total carbon selectivity to the three C₂ hydrocarbons remained >99%, and no deactivation was observed even after reaction for 25 h in this paper. Furthermore, the active site of albite, alkali and alkaline-earth metal site, was determined by the comparison of Pb-introduction and Fe-doping, which provides direction for further modification. Deficiently, the specific adsorption and decomposition processes of methane on albite surface have not been studied owing to the limitations of study conditions. The finding opens up new possibilities for fundamental studies of direct, non-oxidative conversion of methane, the main component of natural gas. It is anticipated that combining a catalyst such as this one with an efficient reactor technology may enable the development of methane-based routes to transform C₂ hydrocarbons into high-value-added chemicals.

Acknowledgements

This work was financially supported by the National Transformation Program for Agricultural Science and Technology (grant number 2012GB2G200469) and Postgraduate Innovation Fund Project by Southwest University of Science and Technology (grant number 17ycx008).

Supplementary Information

Supplementary material includes Figs. S1 and S2 as described in the text, which include XRD patterns of albite before and after calcination, and the fixed-bed flow reactor for NOCM utilized in this paper.

Conflict of Interest

The authors declare that they have no conflict of interest.

References

- [1] Gholipour, Z.; Malekzadeh, A.; Hatami, R.; Mortazavi, Y.; Khodadadi, A.J. *Nat. Gas Chem.* **2010**, 19, 35–42.
- [2] Holmen, A. *Catal. Today* **2009**, 142, 2–8.
- [3] Yuliati, L.; Hattori, T.; Itoh, H.; Yoshida, H. *J. Catal.* **2008**, 257, 396–402.
- [4] Radoiu, M.-T.; Chen, Y.G.; Depew, M.C. *Appl. Catal. B* **2003**, 43, 187–193.
- [5] Gharibi, M.; Zangeneh, Y.; Yaripour, F.T.F.; Sahebdehfar, S. *Appl. Catal. A* **2012**, 443–444, 8–26.
- [6] Tang, P.; Zhu, Q.J.; Wu, Z.X.; Ma, D. *Energy Environ. Sci.* **2014**, 7, 2580–2591.
- [7] Fleischer, V.; Littlewood, P.; Parishan, S.; Schomacker, R. *Chem. Eng. J.* **2016**, 306, 646–654.
- [8] Alexiadis, V.I.; Thybaut, J.W.; Kechagiopoulos, P.N.; Chaar, M.; Van Veen, A.C.; Muhler, M.; Marin, G.B. *Appl. Catal. B* **2014**, 150–151, 496–505.
- [9] Guéret, C.; Daroux, M.; Billaud, F. *Chem. Eng. Sci.* **1997**, 52, 815–827.
- [10] Keramiotis, C.; Vourliotakis, G.; Skevis, G.; Founti, M.A.; Esarte, C.; Sánchez, N.E.; Miller, A.; Bilbao, R.; Alzueta, M.U. *Energy* **2012**, 43, 103–110.
- [11] Holmen, A.; Olsvik, O.; Rokstad, O. A. *Fuel Process Technol.* **1995**, 42, 249–267.
- [12] Fau, G.; Gascoin, N.; Steelant, J.J. *Anal. Appl. Pyrol.* **2014**, 108, 1–11.
- [13] Belgued, M.; Pareja, P.; Amariglio, A.; Amariglio, H. *Nature* **1991**, 352, 789–790.
- [14] Liu, S.Y.; Mei, D.H.; Shen, Z.; Tu, X.J. *Phys. Chem. C* **2014**, 118, 10686–10693.
- [15] Nahreen, S.; Praserthdam, S.; Beltran, S.P.; Balbuena, P.B.; Adhikari, S.; Gupta, R.B. *Energy & Fuels* **2016**, 30, 2584–2593.
- [16] Guzzi, L.; Sarma, K.V.; Borkó, L. *Catal. Lett.* **1996**, 39, 43–47.
- [17] Guzzi, L.; Sarma, K.V.; Borkó, L. *React. Kinet. Catal. Lett.* **1999**, 68, 95–104.

- [18] Guzzi, L.; Sarma, K.V.; Borkó, L. *J. Catal.* **1997**, 167, 495–502.
- [19] Bazin, D.; Borkó, L.; Koppány, Zs.; Kovács, I.; Stefler, G.; Sajó, L.I.; Schay, Z.; Guzzi, L. *Catal. Lett.* **2002**, 84, 169–182.
- [20] Gerceker, D.; Motagamwala, A.H.; Rivera-Dones, K.R.; Miller, J.B.; Huber, G.W.; Mavrikakis, M.; Dumesic, J.A. *ACS Catal.* **2017**, 7, 2088–2100.
- [21] Moya, S.F.; Martins, R.L.; Ota, A.; Kunkes, E.L.; Behrens, M.; Schmal, M. *Appl. Catal. A* **2012**, 411–412, 105–113.
- [22] Moya, S.F.; Martins, R.L.; Schmal, M. *Appl. Catal. A* 2011, 396, 159–169.
- [23] Borkó, L.; Guzzi, L. *Top Catal.* **2006**, 39, 35–43.
- [24] Szeto, K.C.; Norsic, S.; Hardou, L.; Le Roux, E.; Chakka, S.; Thivolle-Cazat, J.; Baudouin, A.; Papaioannou, C.; Basset, J.M.; Taoufik, M. *Chem. Commun.* **2010**, 46, 3985–3987.
- [25] Xu, Y.D.; Bao, X.H.; Lin, L.W. *J. Catal.* **2003**, 216, 386–395.
- [26] Soulivong, D.; Norsic, S.; Taoufik, M.; Copéret, C.; Thivolle-Cazat, J.; Chakka, S.; Basset, J. M.; *Am. Chem. Soc.* **2008**, 130: 5044–5045.
- [27] Lin, X.F.; Xi, Y.Y.; Zhang, G.D.; Phillips, D.L.; Guo, W.Y. *Organometallics* **2014**, 33, 2172–2181.
- [28] Guo, X.G.; Fang, G.Z.; Li, G.; Ma, H.; Fan, H. J.; Yu, L.; Ma, C.; Wu, X.; Deng, D.; Wei, M.; Tan, D.; Si, R.; Zhang, S.; Li, J.; Sun, L.; Tang, Z.; Pan, X.; Bao, X. *Science* **2014**, 344, 616–619.
- [29] Pelte, S.; Flamant, G.; Flamand, R.; Gauthier, D.; Beche, E.; Berjoan, R.; *Miner. Eng.* **2000**, 13, 609–622.
- [30] Baur, W.H.; Joswig, W.; Müller, G.J. *Solid State Chem.* **1996**, 121, 12–23.
- [31] Souza, S.D.O.; Costa, S.S.L.D.; Santos, D.M.; Pinto, J.D.S.; Garcia, C.A.B.; Alves, J.D.P.H.; Geovanny, R. *Spectrochim Acta. B* **2014**, 96, 1–7.
- [32] Caravaca, A.; Lucas-Consuegra, A.D.; González-Cobos, J.; Valverde, J.L.; Dorado, F. *Appl. Catal. B* **2012**, 113–114, 192–200.
- [33] Caravaca, A.; Ferreira, V. J.; Lucas-Consuegra, A.D.; Figueiredo, J.L.; Faria, J.L.; Valverde, J.L.; Dorado, F. *Int. J. Hydrogen Energy* **2013**, 38, 3111–3122.
- [34] Coelho, A.; Caeiro, G.; Lemos, M.A.N.D.A.; Lemos, F.; Ramôa Ribeiro F. *Fuel* **2013**, 111, 449–460.

- [35] Zhao, G.B.; John, Sani; Zhang, J.J.; Wang, L.N. ; Muknahallipatna, S.; Hamannb, J.C.; Ackerman, J.F.; Argyle, D.M.; Plumb, O. A. *Chem. Eng. J.* **2006**, 125, 67–79.
- [36] Deubener, J.; Sternitzke, M.; Müller, G. *Amer. Mineral* **1991**, 76, 1620–1627.
- [37] Liu, R.; Lu, A. H.; Qin, S. *Acta Geol Sin (English Edition)* **2006**, 80, 175–179.
- [38] Tatum, S.H.; Kinoshita, A.; Fukumoto, M.E.; Courriol, L.C.; Kassab, L.R.P.; Baffa, O.; Munita, C.S. *Appl. Radiat. Isot.* **2005**, 62, 231–236.
- [39] Calis, G.; Frenken, P. *Zeolites* **1987**, 7, 319–326.
- [40] Chou, B.; Tsai, J.L.; Cheng, S. *Micropor. Mesopor. Mat.* **2001**, 48, 309–317.
- [41] Farquhar, M.L.; Vaughan, D.J.; Hughes, C.R.; Charnock, J.M.; England, K.E.R.; *Geochim. Cosmochim. Acta.* **1997**, 61, 3051–3064.
- [42] Seyama, H.; Soma, M.J. *Electron, Spectrosc, Relat, Phenom.* **1987**, 42, 97–101.
- [43] Tempelman, C.H.L.; Rodrigues, V.O.; Eck, E.R.H.; Magusin, P.C.M.M.; Hensen, E.J.M. *Micropor. Mesopor. Mat.* **2015**, 203, 259–273.
- [44] Ismagilov, Z.R.; Matus, E.V.; Tsikoza, L.T. *Energy Environ. Sci.* **2008**, 1, 526–541.
- [45] Wang, G.W.; Jin, Y.; Liu, G.J.; Li, Y.D. *Energy & Fuels* **2013**, 27, 4448–4456.
- [46] Fakeeha, A.H.; Ibrahim, A.A.; Naeem, M.A.; Khan, W.U.; Abasaheed, A.E.; Alotaibi, R.L. *Catal. Sustain. Energy* **2015**, 2, 71–82.
- [47] Ashik, U.P.M.; Wan Daud, W.M.A.; Hayashi, J.I. *Renew. Sustain. Energy Rev.* **2017**, 76, 743–767.